Orbitally driven insolation forcing on Holocene climate trends: Evidence from alkenone data and climate modeling

Stephan J. Lorenz,[1,2] Jung-Hyun Kim,[3,4] Norel Rimbu,[5] Ralph R. Schneider,[6] and Gerrit Lohmann[5,7,8]

Received 26 February 2005; revised 26 July 2005; accepted 2 November 2005; published 20 January 2006.

[1] A global spatial pattern of long-term sea surface temperature (SST) trends over the last 7000 years is explored using a comparison of alkenone-derived SST records with transient ensemble climate simulations with a coupled atmosphere-ocean circulation model under orbitally driven insolation forcing. The spatial trend pattern both in paleo-SST data and in model results shows pronounced global heterogeneity. Generally, the extratropics cooled while the tropics experienced a warming during the middle to late Holocene. We attribute these divergent Holocene climate trends to seasonally opposing insolation changes. Furthermore, climate mode changes similar to the Arctic/North Atlantic Oscillation are superimposed on the prevalent pattern. It is concluded that nonlinear changes in the entire seasonal cycle of insolation played a dominant role for the temporal evolution of Holocene surface temperatures. For understanding of marine proxy data, apart from the dominance of summer insolation in high latitudes, a notable shift in the maximum insolation of the year in low latitudes has to be taken into account, which may influence timing of phytoplankton production and thus alters the seasonal origin of temperature signals recorded in the proxies.

Citation: Lorenz, S. J., J.-H. Kim, N. Rimbu, R. R. Schneider, and G. Lohmann (2006), Orbitally driven insolation forcing on Holocene climate trends: Evidence from alkenone data and climate modeling, *Paleoceanography*, *21*, PA1002, doi:10.1029/2005PA001152.

1. Introduction

[2] The changes in the seasonal cycle of solar irradiance at the outer boundary of the atmosphere, caused by the varying parameters of the Earth's orbit around the Sun (astronomical forcing or orbitally driven insolation forcing), is one of the most prominent forcing mechanisms for long-term climate change. The insolation changes at northern high latitudes during boreal summer have been regarded as the dominant external forcing for glacial-interglacial climate changes during the Quaternary ("Milankovitch forcing") [*Milankovitch*, 1941; *Hays et al.*, 1976; *Imbrie et al.*, 1992].

[3] The relative role of the effect of orbital forcing on Holocene climate change is, however, not well known. The climate of the last glacial, preceding the Holocene, was periodically punctuated by a series of abrupt climate changes, known as Dansgaard-Oeschger events [*Broecker*, 1998; *McManus et al.*, 1999]. In contrast, the Holocene trends in sea level [*Fairbanks*, 1989] as well as in the oxygen isotope composition of polar ice sheets [*Grootes et al.*, 1993] imply that the Holocene climate was relatively stable when compared to the last glacial. *Broecker* [1998] stated that neither the sea level nor the Greenland ice $\delta^{18}O$ record show a tendency toward the cooling expected in response to the Holocene decrease in boreal summer insolation in high northern latitudes. To challenge this view, we here show spatially varying patterns of long-term surface temperature trends for the Holocene. We address the role of orbital forcing during the Holocene based on globally distributed alkenone-derived sea surface temperature (SST) records in comparison with transient climate simulations using a coupled atmosphere-ocean general circulation model (AOGCM).

[4] The majority of AOGCMs has been utilized to quantitatively evaluate the magnitude of future climate change. Their results served as a scientific basis for the third assessment report of the *Intergovernmental Panel on Climate Change* [2001]. Validation of these models by simulating different climate states is essential for understanding the sensitivity of the climate system to both natural and anthropogenic forcing.

[5] Up to now, the validation of AOGCMs has primarily been based on the comparison of results reproducing the instrumental climate record of the last 150 years. However, the instrumental period coincides with that of strong an-

[1] Modelle und Daten, Max-Planck-Institut für Meteorologie, Hamburg, Germany.
[2] Now at Meteorologisches Institut, Universität Hamburg, Hamburg, Germany.
[3] Fachbereich 5, Geowissenschaften, Universität Bremen, Bremen, Germany.
[4] Now at Centre de Formation et de Recherche sur l'Environnement Marin, CNRS-UMR 5110, Université de Perpignan, Perpignan, France.
[5] Alfred-Wegener-Institut für Polar- und Meeresforschung, Bremerhaven, Germany.
[6] Institut für Geowissenschaften, Christian-Albrechts-Universität zu Kiel, Kiel, Germany.
[7] Fachbereich Physik/Elektrotechnik, Universität Bremen, Bremen, Germany.
[8] DFG-Forschungszentrum Ozeanränder, Universität Bremen, Bremen, Germany.

0883-8305/06/2005PA001152$12.00

thropogenic impacts. Therefore it is necessary to test the results of AOGCMs beyond this period (at least the Holocene) in order to identify coherent natural climate variations and their underlying mechanisms and hence to properly address the question of anthropogenic influence on climate.

[6] Recent modeling efforts to simulate Holocene climate changes using coupled AOGCMs [*Hewitt and Mitchell*, 1998; *Liu et al.*, 1999; *Voss and Mikolajewicz*, 2001; *Kitoh and Murakami*, 2002; *Liu et al.*, 2003] assume that the atmosphere-ocean system is in equilibrium with the external forcing. Modeling studies based on simulations with a single model [*Hewitt and Mitchell*, 1998; *Lohmann and Lorenz*, 2000], and model-model comparisons [*Guiot et al.*, 1999; *Braconnot et al.*, 2002], as well as data-model syntheses [*Kohfeld and Harrison*, 2000; *Texier et al.*, 2000] have mainly been undertaken in the framework of the Paleoclimate Modeling Intercomparison Project (PMIP) [*Joussaume and Taylor*, 2000]. Transient simulations of the Holocene without the assumption of an equilibrium climate and including orbital forcing were predominantly performed utilizing models of intermediate complexity (for a summary, see *Claussen et al.* [2002]). Some of the simulations with these models [*Bertrand et al.*, 2002; *Weber et al.*, 2004; *Renssen et al.*, 2005] confirmed the influence of insolation changes as well as the importance of including ocean feedbacks.

[7] In this study, the ensemble simulations were conducted with a state-of-the-art fully coupled AOGCM, the ECHO-G [*Legutke and Voss*, 1999], where an acceleration technique for the orbital forcing has been employed [*Lorenz and Lohmann*, 2004]. The ECHO-G model has participated in the "Coupled Model Intercomparison Project" (CMIP) and will participate with other AOGCMs in the next set of Intergovernmental Panel on Climate Change (IPCC) experiments for the Fourth Assessment Report of the IPCC, planned for 2007.

[8] Recently, on the basis of the control run of the ECHO-G model in comparison with alkenone-derived SST records, internal processes which underlay teleconnections between the North Atlantic and the North Pacific [*Kim et al.*, 2004] as well as between the North Atlantic and tropical oceans [*Rimbu et al.*, 2004] were investigated on centennial to millennial timescales. Here we focus on the effect of the seasonal insolation changes on heterogeneous Holocene surface temperature trends as observed in both globally distributed alkenone-derived SST records and transient ensemble simulations with the ECHO-G model.

[9] Conforming with the PMIP definition of the middle Holocene time slice, which was chosen to be 6000 years before present (kyr B.P. in the following), this data-model comparison study concentrates on the middle to late Holocene. The last 7000 years can be regarded as relatively stable compared to former eras, because these were probably excluded from severe shifts in the atmosphere-ocean system [*Grootes et al.*, 1993; *McManus et al.*, 2004].

[10] Since the development of the unsaturated alkenone index as a temperature proxy in the late 1980s, the seasonal origin of alkenone-derived temperature signals in different latitudes has been questioned. In high latitudes, maximum phytoplankton coccolithophorid production is observed in summer [*Baumann et al.*, 1997] suggesting that alkenone-derived SSTs should reflect summer temperatures [*Rosell-Melé et al.*, 1995; *Sikes et al.*, 1997]. In contrast, seasonality in phytoplankton production is generally less pronounced in tropical to subtropical regions [*Jickells et al.*, 1996] and alkenone-derived SSTs are more likely to show temperatures close to the annual mean values [*Müller and Fischer*, 2001]. For comparison, our AOGCM results show Holocene climate changes in the seasonal cycle of surface temperatures and can thus provide hints to the seasonal origin of alkenone-derived SST in different latitudes.

[11] The paper is organized as follows. In the next section we start with a discussion of the orbitally driven changes in the seasonal cycle of insolation during the Holocene. Next (section 3) an introduction to the methods is given: the reconstruction of SST records from alkenones, and the AOGCM, including its orbital forcing, the acceleration technique for this forcing, and the model experiments. The long-term Holocene trends in surface temperature of reconstructed data and model results, including analysis of seasonal trends, are then shown (section 4). The dependence of these trends on orbitally driven insolation change and its impact in relation to other forcing and feedback mechanisms is discussed (section 5). Finally, concluding remarks (section 6) are given.

2. Orbitally Driven Insolation Changes During the Holocene

[12] Three main parameters of the Earth's orbit around the Sun control the seasonal distribution of solar radiation at the top of the atmosphere: the eccentricity of the orbit with the Sun in one of the two foci, the time of the Earth's passage through its perihelion, and the tilt of its rotation axis. Long-term variation in these parameters cause the astronomical or "Milankovitch forcing" of the climate system [*Milankovitch*, 1941; *Imbrie et al.*, 1992]. The variation can easily be calculated with sufficient accuracy using the algorithm of *Berger* [1978]. Newer calculations span much longer timescales, beyond millions of years [*Laskar et al.*, 2004], or take into account short-term variability [*Loutre et al.*, 1992], which is far beyond the requirements of our model experiments.

[13] The eccentricity (ϵ) has cycles with periods near 100,000 years and affects the annual mean top-of-atmosphere insolation on the entire Earth by much less than 0.1% during the Holocene. The amplitude of the precession parameter e, where $e = \epsilon \sin(\lambda)$ with λ the longitude of the perihelion measured from the vernal equinox ($\approx 282^\circ$ today, with perihelion at the beginning of January) is modulated by the eccentricity and has cycles with periods near 20,000 years. It determines the time of the year when the insolation of the whole Earth is at maximum. The third parameter, the Earth's axis tilt (obliquity) has a main long-term cycle with a period near 40,000 years and governs the amplitude of the seasonal cycle of both hemispheres.

[14] During the Holocene, the seasonal distribution of Earth's top-of-atmosphere insolation varied considerably

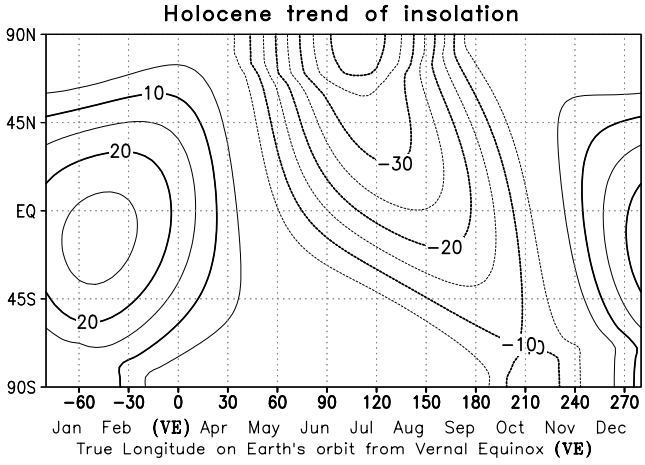

Figure 1. Latitudinal distribution through the year, with respect to the Earth's orbital longitude measured from vernal equinox (noted as "true longitude" and "VE"), of the today minus 7 kyr B.P. difference in top-of-atmosphere insolation (W m^{-2}), calculated after *Berger* [1978]. Note that, for comparison with sea surface temperature (SST) trends, this is equivalent to the linear trend in insolation over the last 7000 years.

because of precession and obliquity cycles. During the last 7000 years, these cycles caused a shift of perihelion from September ($\lambda = 164°$) to January ($\lambda = 282°$) and a decrease in the tilt of the Earth's axis from 24.2° to 23.4°. The resulting radiative changes over the last 7000 years are displayed in Figure 1. It shows the latitudinal distribution through the year of the today minus 7 kyr B.P. difference in top-of-atmosphere insolation. The most pronounced radiative changes were a decrease in the boreal summer insolation (June-July-August (JJA)) of more than 30 W m^{-2} in the northern middle to high latitudes accompanied by an increase in the boreal winter insolation (December-January-February (DJF)) of about 25 W m^{-2} in the low latitudes (Figure 1).

[15] Along with the seasonal changes, the dominant orbital parameter in the tropics, the precession parameter, is able to cause a shift in the occurrence of the maximum insolation throughout the year. Equatorial insolation is generally highest during passage through the equinoxes, when the Sun is at the zenith. Equatorward of the two tropics the Sun reaches the zenith two times a year resulting in a characteristic semiannual cycle of tropical insolation. The precession cycles can vigorously modulate this seasonal cycle. For example, in the zonal band between 10°N and the equator, insolation at present has nearly equal maxima in March and September (Figure 2a). In contrast, during the middle Holocene insolation was at its maximum in September, when the distance to the Sun was at its minimum and insolation reached 30 W m^{-2} more than during March (Figures 2a and 2b). Therefore, comparing the seasonal cycle of present and middle Holocene insolation, the time when its maximum is reached shifts from the middle of March to the beginning of September (Figure 2a).

3. Data and Methods

3.1. Alkenone-Derived SST Data

[16] For this study, a marine Holocene paleotemperature data set covering all major ocean basins [*Kim and Schneider*, 2004] has been compiled. The data set has been derived from a temperature proxy (alkenones) that is internationally calibrated and standardized among 24 laboratories worldwide [*Rosell-Melé et al.*, 2001]. We consider 46 SST records solely based on the alkenone method as paleothermometry in order to avoid potential biases because of using different SST proxies. The paleotemperature estimates are based on the abundance ratios of long-chain unsaturated

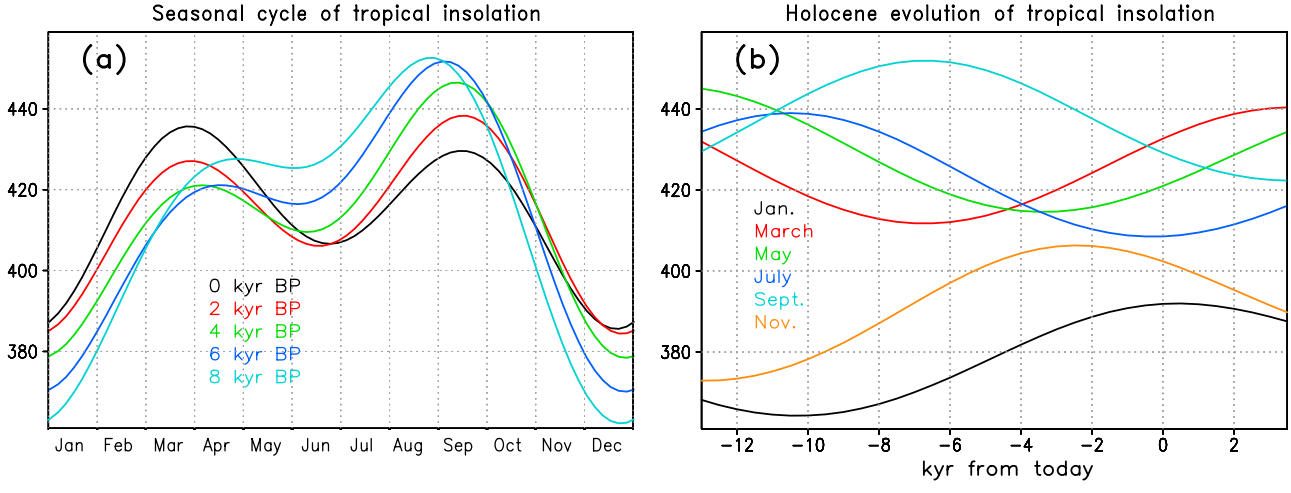

Figure 2. Changes in the seasonal cycle of insolation (W m^{-2}) in the tropics (0°–10°N) during the Holocene (calculated after *Berger* [1978]): (a) seasonal cycle of insolation for five time slices in the Holocene and (b) evolution from the early Holocene into the next millennia of insolation for the tenth day of selected months.

alkenones with two to four double bonds [*Brassell et al.*, 1986; *Prahl and Wakeham*, 1987]. Alkenones are synthesized by the class Prymnesiophyceae of which the coccolithophorids *Emiliania huxleyi* and *Gephyrocapsa oceanica* are the two most common sources of alkenones in contemporary oceans and sediments [*Volkman et al.*, 1980; *Conte et al.*, 1995].

[17] Different alkenone unsaturation indices (U_{37}^{K} or $U_{37}^{K'}$) and calibrations were applied for each alkenone-derived SST record. The errors in alkenone-derived temperature reported for the culture calibration and for a global core top calibration reach ±0.5°C [*Prahl and Wakeham*, 1987] and ±1.5°C [*Müller et al.*, 1998], respectively. Analytical accuracy for each record considered here, however, was better than ±0.3°C [see *Kim and Schneider*, 2004]. The age models of the alkenone-derived SST time series were established mainly by accelerator mass spectrometry (AMS) ^{14}C determinations on planktic foraminifera and by oxygen isotope chronologies. All SST records were from ocean margin sites with sedimentation rates sufficiently high to provide SST records with at least one value per 1000 years. Detailed information on each SST record are given by *Kim and Schneider* [2004], including the original data references. Figure 3 shows 20 examples of alkenone-derived SST records along with their linear regressions and their locations in the map.

3.2. General Circulation Model and Experimental Setup

3.2.1. Coupled Atmosphere-Ocean General Circulation Model

[18] The transient climate simulations were performed with the coupled general circulation model ECHO-G [*Legutke and Voss*, 1999]. The atmospheric part of this model is ECHAM4 [*Roeckner et al.*, 1996], whose prognostic variables are calculated in the spectral domain using a medium resolution (T30), corresponding to a longitude-latitude grid of approximately 3.8° × 3.8° with 19 levels in the vertical. The time step of the atmospheric model is 30 min. The ECHAM4 model is coupled to the HOPE ocean general circulation model [*Wolff et al.*, 1997], which includes a dynamic-thermodynamic sea ice model with snow cover. It is discretized with a horizontal resolution of approximately 2.8° × 2.8° (0.5° resolution in the tropics, 20 vertical levels) and has a time step of two hours. The model utilizes annual mean flux corrections for heat and freshwater. These fluxes are constant in time and have no sources or sinks of energy or mass.

[19] In the ECHO-G model, the calculation of the orbital parameters follows *Berger* [1978]. The atmospheric part of the ECHO-G model, the ECHAM4, has been adapted to account for the different insolation during paleoclimatic time slices [*Lorenz et al.*, 1996]. Moreover, to evaluate the dynamical variation of insolation during the Holocene, the calculation of the orbital parameters is done individually for each simulation year.

3.2.2. Acceleration Technique

[20] We use an acceleration technique implemented into the ECHO-G model to conduct transient simulations over millennia [*Lorenz and Lohmann*, 2004]. To be able to simulate a period of 7000 years with this model, the timescale of the orbital forcing is shortened by an acceleration factor of 100. The underlying assumptions are that the orbital forcing operates on much longer timescales (millennia) than those inherent in the atmosphere including the surface mixed layer of the ocean (months to years), and that climatic changes related to long-term variability of the thermohaline circulation during the time period considered are negligible in comparison with orbitally driven surface temperature variation. With this method, climate trends and feedbacks of the last 7000 years, imposed by the external orbitally driven insolation changes, are represented in the experiments with only 70 simulation years. The experiments with the coupled AOGCM capture the internal variability of the atmosphere-ocean–sea ice system with timescales up to decades.

[21] In line with Holocene reconstructions, additional experiments using an acceleration factor of 10 (700 simulation years) exhibit no change in the simulated meridional overturning circulation during the last 7000 years. Moreover, these experiments demonstrate that the magnitude of orbitally forced Holocene trends is independent of the chosen factor [*Lorenz and Lohmann*, 2004].

3.2.3. Experimental Setup

[22] We performed one simulation of preindustrial climate. Constant greenhouse gas concentrations typical for the preindustrial era at the very end of the Holocene (ca. 1800 A.D.) were prescribed. These have been compiled mainly from ice core records [*Etheridge et al.*, 1996, 1998; *Indermühle et al.*, 1999; *Sowers et al.*, 2003]: 280 ppm CO_2, 700 ppb CH_4, and 265 ppb N_2O. Other boundary conditions (surface background albedo, vegetation ratio, leaf area index, distribution of continents and oceans) were kept constant at their present values throughout the simulation and modern insolation was used. This control experiment was integrated over a total of 3000 model years. The climate state, which becomes relatively stable after 1250 model years [*Lorenz and Lohmann*, 2004], is regarded as the quasi-equilibrium response of the model to preindustrial boundary conditions.

[23] The set of ensemble simulations of the Holocene comprises six model runs, each going through the entire last 9000 years, using an acceleration factor of 100. In order to isolate the orbitally driven insolation effect on the simulated Holocene climate evolution, small changes in greenhouse gases during the Holocene [*Indermühle et al.*, 1999] are ignored and the model is forced only with orbitally varying insolation. Similarly, variations in the Sun's output of radiation (solar constant) as well as reduced insolation due to atmospheric dust loads after volcanic eruptions are not taken into account, since no continuous data apart from the last millennium exist [*Crowley*, 2000].

[24] The Holocene simulations start after year 1250 of the control experiment when the coupled system including the deep ocean is regarded to be in a quasi-equilibrium with the preindustrial boundary conditions and modern insolation. The simulation of the early Holocene (9–7 kyr B.P.) at the beginning of the Holocene experiments is taken as spin-up time for the model to adapt to the nonmodern insolation distribution. The simulation of the subsequent

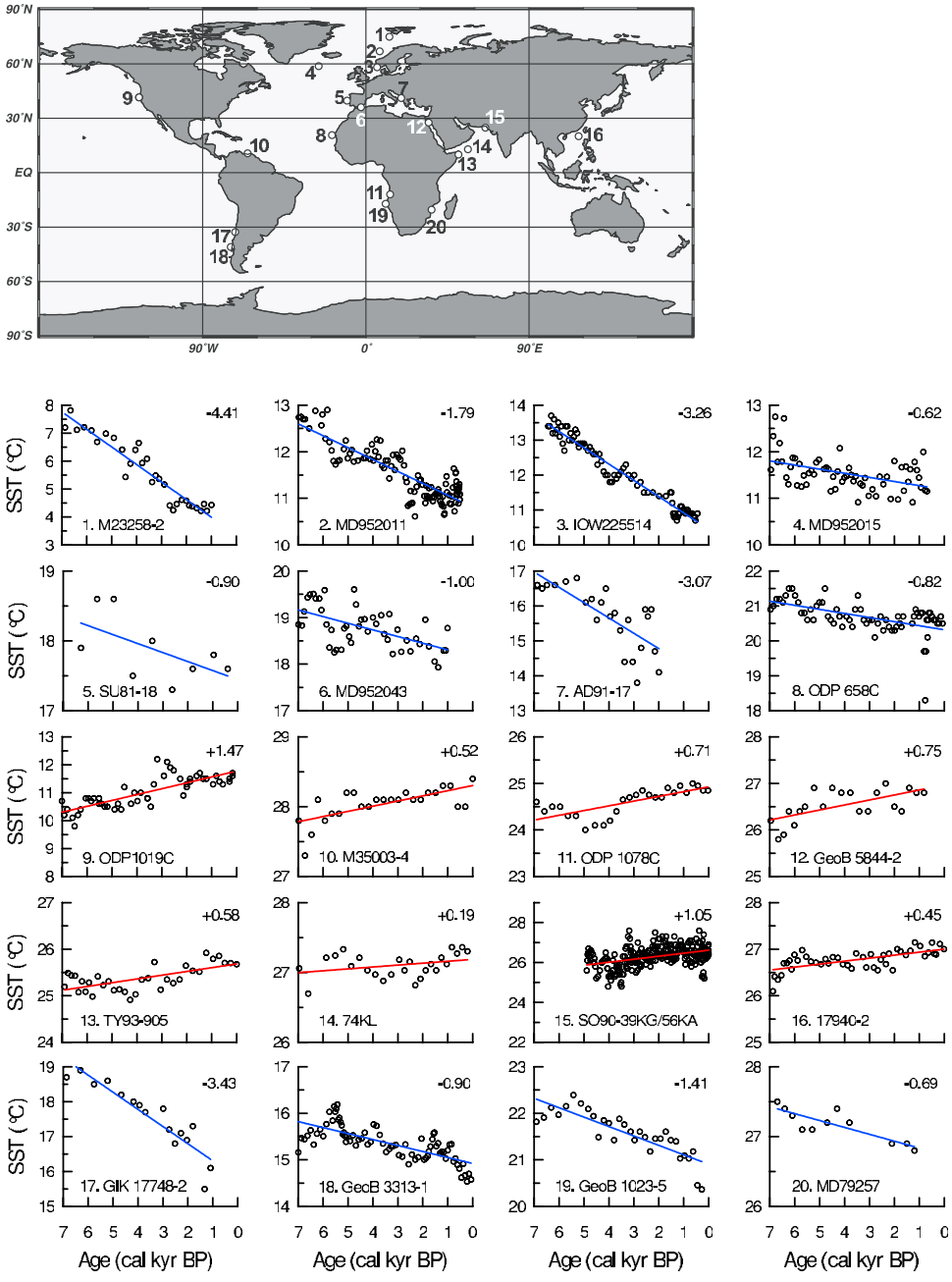

Figure 3. Examples of alkenone-derived SST records (circles) and their linear trends (solid lines) evaluated from 20 cores, whose positions are shown on the map [*Kim and Schneider*, 2004; see also *Kim et al.*, 2004, Table 1]. The magnitude of SST change over the last 7000 years (calendar age) is indicated in the upper right corner of each panel.

period from the middle Holocene into the preindustrial era (7 kyr B.P. to 1800 A.D.) is used for the trend analysis.

4. Long-Term Surface Temperature Trends

[25] In this section the temporal and spatial patterns of long-term surface temperature trends, evaluated from alkenone-derived SST reconstructions and transient general circulation experiments, are compared. We explore the Holocene trends of annual mean temperature, as well as seasonal trends evaluated from the ensemble of model experiments.

4.1. Annual Mean Trends

[26] The alkenone-derived SST records show diverging linear trends over the last 7000 years (Figures 3 and 4a). In general, the extratropics cooled while the tropics experienced a warming or no substantial temperature changes from 7 kyr B.P. to the present. The magnitude varied between -0.62°C and -4.41°C per 7 kyr for the cooling

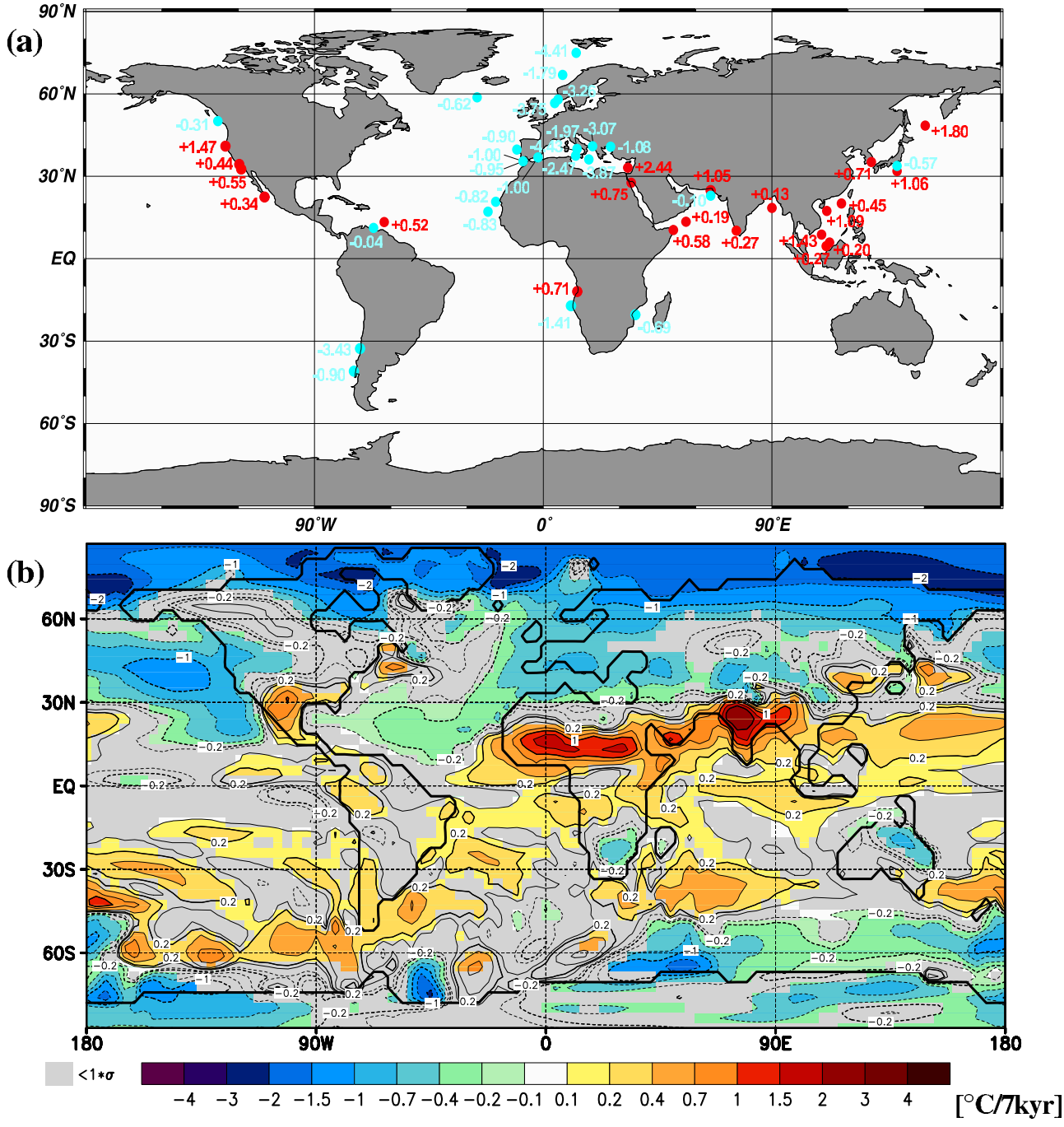

Figure 4. Holocene surface temperature trends derived from alkenone proxies and coupled atmosphere-ocean general circulation model (AOGCM) simulations in °C per 7 kyr: (a) marine sediment core positions and corresponding magnitudes of alkenone-derived SST change over the last 7000 years and (b) spatial distribution of annual mean surface temperature trends from six ensemble simulations, each covering the last 7000 years. Values are sea surface temperature changes over ice-free water and ground, ice, or snow temperatures over continents and ice-covered oceans. Shaded areas represent the regions where the trend does not exceed 1 standard deviation. The continents are shown in the resolution of the atmospheric model.

and between +0.19°C and +1.47°C per 7 kyr for the warming (Figure 3). However, the zonal distribution of SST trends is inhomogeneous, showing east-west variations for the same latitudes and abrupt changes in trends across oceanic frontal systems, e. g., the Angola-Benguela Front in the southeast Atlantic. The leading EOF of SST variability (not shown) describes 58% of the field variance and indicates a spatial pattern similar to the pattern of linear

temperature trend as derived from alkenone-data for the last 7000 years (Figure 4a).

[27] The described coupled AOGCM experiments reveal pronounced annual surface temperature trends over the last 7000 years. The temperature trend pattern is evaluated from the uppermost surface temperature in the model: SST over ice-free water, and ground (bare or vegetated land), ice (sea ice or land ice), or snow temperature (snow covered areas) wherever appropriate (Figure 4b). A continuous cooling in the northern middle to high latitudes and in the southern high latitudes was accompanied by a warming in the tropics as well as in the southern midlatitudes. The simulated cooling exceeds 2°C in the Arctic and 1°C over the Pacific and northern Europe. A transient warming is most pronounced in the northern low latitudes, especially over the continents, where the low heat capacity of soil compared to ocean amplifies the surface temperature trend. It exceeds 1°C over North Africa, the Arabian Peninsula and the Indian subcontinent. Off the continents, the warming reaches 0.5°C over the eastern tropical Atlantic, the northern Indian Ocean, and the western tropical Pacific. The surface temperature trends are not zonally homogeneous over a whole basin: for example, in the northern midlatitudes, there is a warming in the western Atlantic and Pacific, while their eastern counterparts experienced a cooling (Figure 4b).

[28] The simulated surface temperature trends are similar to the linear trends in the alkenone-derived SSTs in the northern extratropics as well as in the tropics. In general, the amplitudes of SST trends from the simulations are smaller compared to those of alkenone-derived SSTs. A significant discrepancy between alkenone-derived SST data and model results occurs off Chile and Namibia. Generally, in the coastal regions around South America and southern Africa, reconstructed SST trends are negative whereas simulated trends are positive (South America) or uncertain in sign (southern Africa).

4.2. Seasonal Trends

[29] Since seasonality cannot be resolved by the alkenone method, we concentrate on the model results and examine the trends over the last 7000 years for the boreal summer (JJA) and winter (DJF) seasons, respectively (Figure 5). In the boreal summer (Figure 5a), there is a Holocene cooling mainly over the continents of the Northern Hemisphere (1°C–3°C), which is in line with the reduction of insolation by 15 to 30 W m^{-2} north of 30°N. The cooling is less pronounced in the North Atlantic and the North Pacific and large parts of the Southern Hemisphere continents.

[30] In the boreal winter (Figure 5b), the continents generally exhibit a pronounced warming of 1°C–2°C. This signal is not only significant in the tropics, where it follows the increase in insolation (Figure 1), but also in the midlatitudes. Over the oceans, the trend patterns are much less significant, although they do show a warming over the central and northwest Pacific Oceans as well as off West Africa. Over the North Atlantic a dipole structure is found with a warming in the eastern and a cooling in the western part and over Europe. Over the whole ocean, cooling is located mainly in the Arctic, the northeast Atlantic and Pacific, and parts of the Southern Ocean.

[31] Furthermore, we look now at the trends of the simulated maximum and minimum monthly temperature: from the ensemble mean of the six Holocene experiments we extract the coldest and warmest months of each simulated year. Then the trend at each of the grid points is evaluated. Thus the temperature trend from the warmest or coldest month in each year is computed locally, no matter which month this is. With this method, the trends reflect the characteristic change of the local summer or local winter at each grid point in Figures 6a and 6b, respectively. For example, in high latitudes, Figure 6a shows the local summer of both hemispheres combined. In the tropics, with its semiannual cycle of insolation, the extremes of surface temperature trends also include the precession effect of a Holocene shift in the seasonal cycle of insolation.

[32] The most significant trends are found for local summer (Figure 6a). Both hemispheres show opposite signals with a strong temperature decrease (1°C–4°C) in the Northern Hemisphere and an increase in the Southern Hemisphere. This can be attributed to the precessional shift of perihelion from September in the middle Holocene to January today: over the last 7000 years, the reduction in insolation during the JJA season exceeded 20 W m^{-2} in the Northern Hemisphere, while simultaneously almost the whole Earth experienced an insolation increase during the DJF season (Figure 1). For this reason today the maximum daily mean insolation anywhere on Earth is at the South Pole (560 W m^{-2}) at the winter solstice (austral summer), when the distance to the Sun is near its minimum. In the Northern Hemisphere, the trend pattern of the local winter (Figure 6b) is very close to the pattern of the DJF season (Figure 5b).

5. Discussion

5.1. Orbital Forcing of Surface Temperature Trends

[33] The global spatial pattern of alkenone-derived and modeled SST trends during the last 7000 years can be summarized by an overall decrease in the extratropics accompanied by a slight increase in the tropics. The cooling trends observed in the northern middle to high latitudes concur with a previous study [*Marchal et al.*, 2002], which showed a long-term cooling in the northeastern Atlantic and the western Mediterranean during the Holocene. However, small-scale changes of sign in alkenone-derived SST trends occur off the coasts of Caribbean South America, southwest Africa, and Japan. These changes may be related to regional patterns across oceanic frontal systems. Such relatively small-scale patterns are difficult to reproduce accurately using a medium-resolution global climate model under generalized forcing.

[34] The zonally averaged model results suggest that the strongly decreasing boreal summer insolation induced a progressive surface temperature cooling of 1.4°C in the northern middle to high latitudes (north of 30°N; Figure 5a) [see *Lorenz and Lohmann*, 2004]. During boreal winter (DJF) in low latitudes (30°N to 30°S), a rise in simulated surface temperature (Figure 5b) amounts to 0.4°C in the zonal mean (not shown) and is in concor-

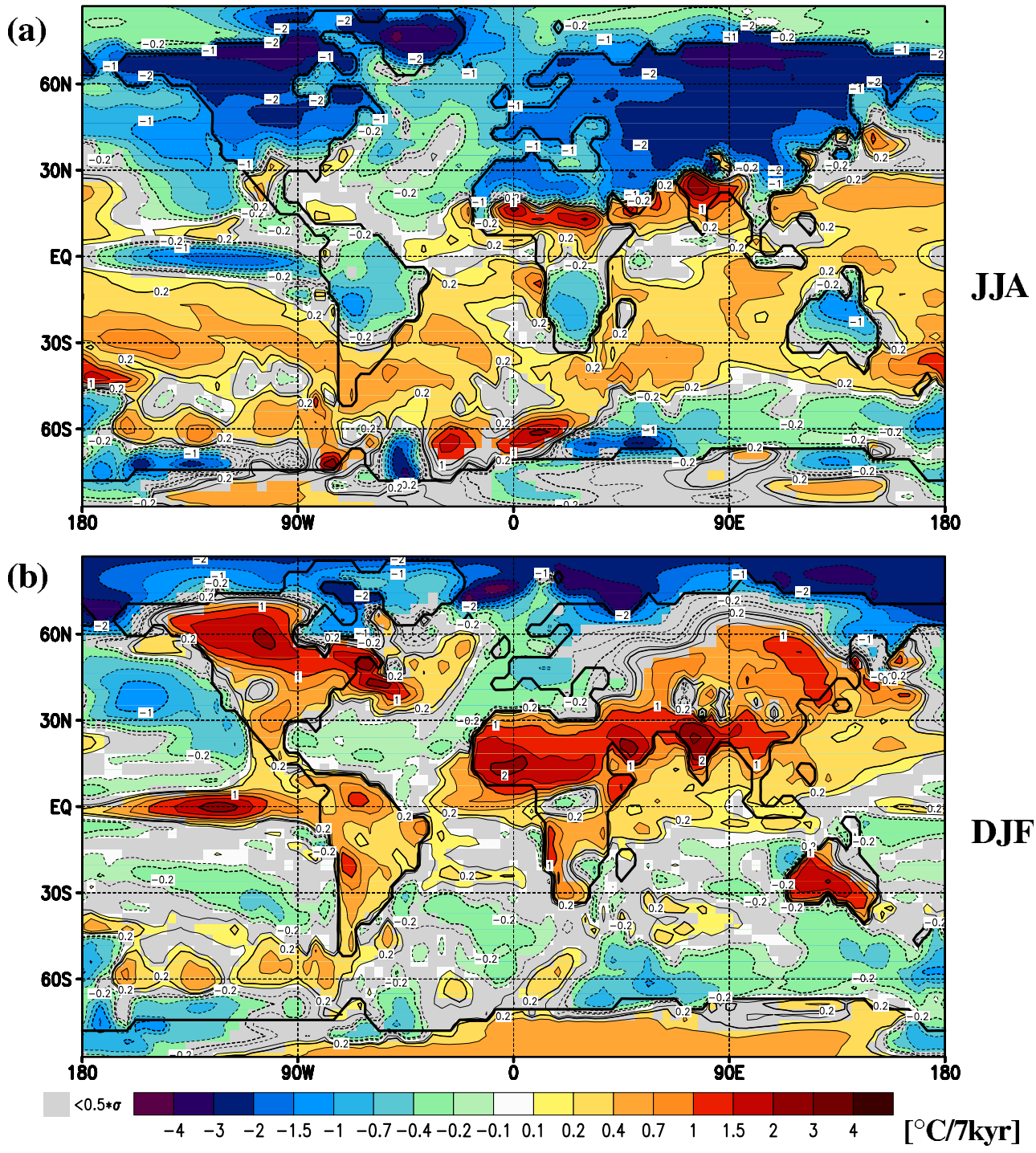

Figure 5. Simulated seasonal mean surface temperature trends during the Holocene (in °C per 7 kyr): (a) boreal summer, June–July–August (JJA), and (b) boreal winter, December–January–February (DJF). Shaded areas represent the regions where the trend does not exceed 1/2 standard deviation. See Figure 4b for further details.

dance with the increasing tropical insolation in that season (Figure 1).

[35] The seasonally averaged model results imply that the DJF warming slightly exceeded the JJA cooling in the tropics, resulting in a moderate warming. This suggests that surface temperatures responded nonlinearly to the seasonal signal of orbitally driven insolation over the last 7000 years. The main result of colder tropics and warmer extratropics for the middle Holocene climate compared to the present is in overall agreement with previous modeling studies based

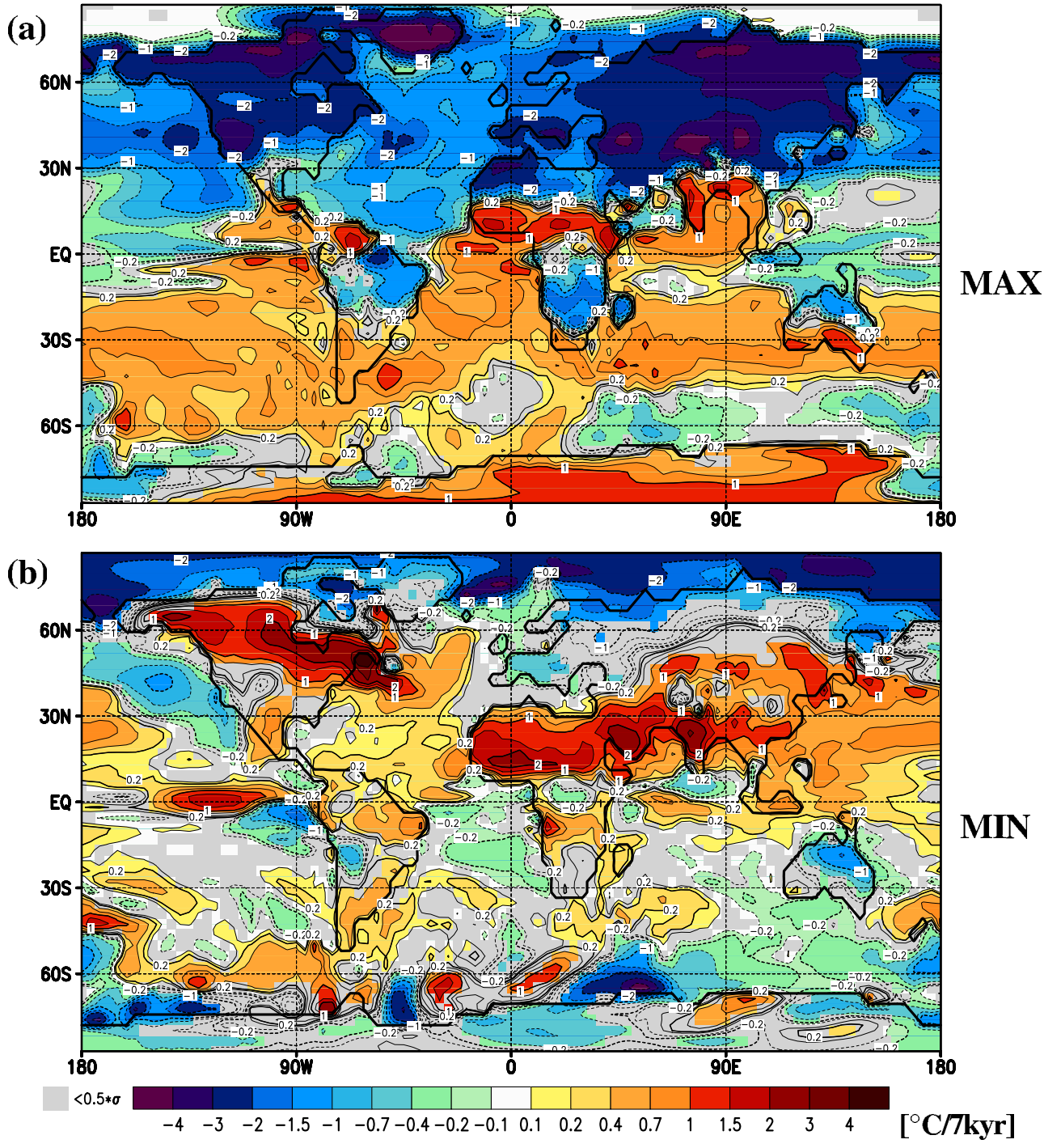

Figure 6. Simulated surface temperature trends (in °C per 7 kyr) of the (a) warmest (local summer) and (b) coldest (local winter) month of the year during the Holocene. See Figure 4 and text for further details.

on the time slice approach [*Hewitt and Mitchell*, 1998; *Voss and Mikolajewicz*, 2001; *Kitoh and Murakami*, 2002; *Liu et al.*, 2003]. However, besides the transient simulations performed here, we analyzed the temperature trends for different seasons: the boreal summer and boreal winter as well as the warmest (local summer) and coldest (local winter) months, respectively.

[36] The larger amplitudes of the simulated trends during the boreal summer (Figure 5a), in particular for the North Atlantic and Mediterranean, are in better agreement with the alkenone-derived SSTs (Figure 4a) than the simulated relatively weak annual mean trends (Figure 4b). Off the west coast of the North Pacific, larger positive trends are found, whereas in the eastern

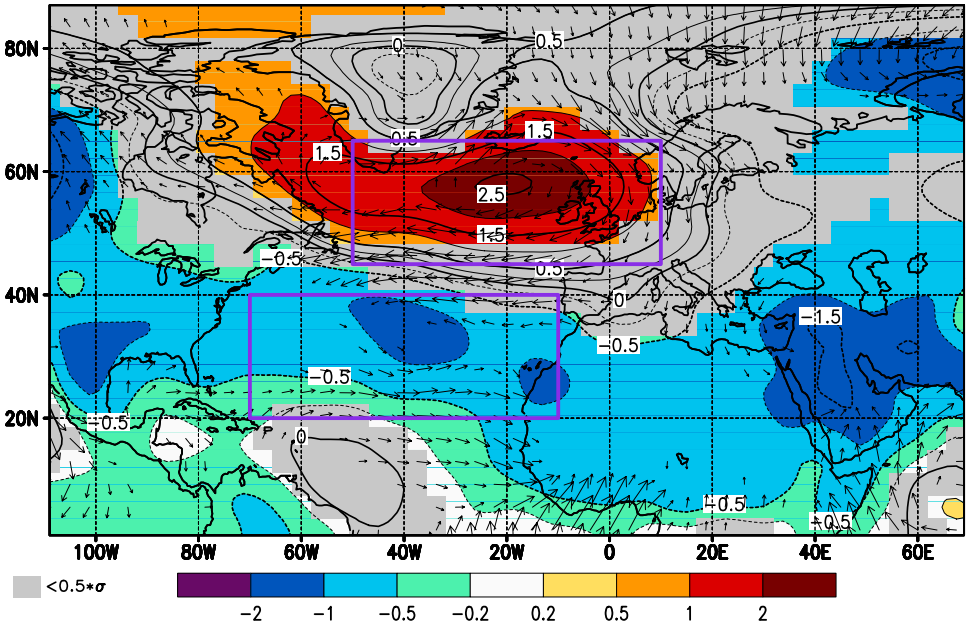

Figure 7. Simulated trend of boreal winter (DJF) sea level pressure from the six ensemble Holocene (7 kyr B.P. to present) simulations. Shaded areas represent the regions where the trend does not exceed 1/2 standard deviation. The rectangles indicate two regions in the North Atlantic, between which the meridional pressure difference for Figure 8 is calculated. Additionally, 10 m wind vectors of the 7000 years trend are shown but only where their magnitude exceeds 0.3 m s^{-1}.

part the mismatches between data and model results remain for the boreal winter.

[37] Analyzing the trends of the maximum and minimum monthly surface temperature, we note a striking agreement in sign and amplitude of the simulated trends of the local summer (Figure 6a) with the alkenone-derived SST trends in the whole North Atlantic (around 1°C cooling) and Mediterranean (2°C–3°C cooling). This may be taken as evidence that alkenone-derived temperature signals in the northern extratropics are more likely to stem from summer conditions, when the phytoplankton blooming occurs, than to reflect annual mean temperature. It is likely that coccolithophorid blooming during the early to middle Holocene took place in late summer (September), when high latitude insolation was at its maximum.

[38] Interestingly, even in the tropics, there is a match of the alkenone-derived SST trend pattern with that of local summer, with a decrease of 1°C in the tropical Atlantic and an increase of around 0.5°C–1°C in the northern Indian Ocean and the China Sea. For these regions, this pattern match is better than with any other of the simulated seasonal and annual mean surface temperature trends.

[39] Although the seasonal cycle of SST in the tropics is small, phytoplankton production is not constant throughout the year. It is reasonable that a change of seasonal insolation on the order of 10% is able to impact marine biological productivity. If the alkenone production is thought to be highest during the month with the warmest water temperature in the mixed layer, then the resemblance of reconstructed trends with the simulated trends of local summer can be taken as an indication that the time of maximum production may have changed with the insolation signal.

5.2. The Arctic/North Atlantic Oscillation

[40] The Holocene tropical warming and extratropical cooling observed in both the alkenone-derived SST records and in the model results was accompanied by a weakening of the Atlantic midlatitude zonal surface temperature contrast, mainly in boreal winter (Figure 5b): A cooling over the eastern North Atlantic opposes a warming over the western North Atlantic and eastern part of North America.

[41] Also in boreal winter in the North Atlantic, we find a notable Holocene decrease in sea level pressure difference between the high latitude (Icelandic) low and the subtropical (Azores) high by more than 3 hPa (Figure 7). We relate the decrease in east-west surface temperature difference in the North Atlantic with a Holocene weakening of the midlatitude atmospheric circulation pattern that resembles the modern Arctic Oscillation/North Atlantic Oscillation (AO/NAO) [*Hurrell*, 1995; *Thompson and Wallace*, 1998]. This pattern, also known as the northern annular mode, is the dominant winter circulation mode in the extratropics of the Northern Hemisphere, in particular in the North Atlantic realm [*Thompson and Wallace*, 2001]. The time series of the pressure difference (Figure 8) between the two large-scale areas outlined in Figure 7 indicates a decrease of the Atlantic meridional pressure gradient by 2 hPa over the last 7000 years. This led to considerable changes in surface winds, exceeding 1 m s^{-1}

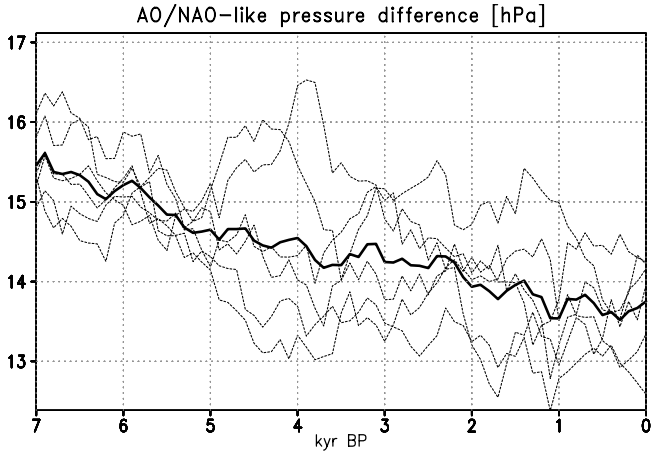

Figure 8. Meridional pressure gradient between the two regions shown in Figure 7. It is interpreted as the evolution of the Arctic Oscillation/North Atlantic Oscillation (AO/NAO) index over the last 7000 years: the difference in mean sea level pressure during boreal winter (DJF) between a low-latitude/high-pressure box (longitude 50°W to 10°E, latitude 45°N to 65°N) minus a high-latitude/low-pressure box (longitude 70°W to 10°W, latitude 20°N to 40°N) in the North Atlantic. The thick line depicts the ensemble mean of the six Holocene experiments, which are shown individually as thin dashed lines. A 21-year running mean is used as a low-pass filter for all experiments.

(see Holocene wind change vectors in Figure 7) and including reduced westerly winds in the Atlantic at 45°N (less advection of warm air into Europe), southerly wind components in Central Europe (advection of cold air), and northerly anomalous winds into Africa and the Red Sea (advection of warm air). These changes are typical of a decrease in AO/NAO. The reduction of this mode leads to a characteristic dipole structure, with cooling over Europe and warming in the subtropics, mainly in the eastern Mediterranean Sea and the Red Sea [e.g., *Felis et al.*, 2000]. A Holocene temperature decrease over Europe in winter is contrary to enhanced insolation from the orbital changes (Figure 1). The simulated European winter cooling is in line with a recent study analyzing alkenone-derived Holocene SST records and instrumental data from the North Atlantic and Mediterranean [*Rimbu et al.*, 2003] as well as a study analyzing the circulation pattern in the Nordic Seas [*Lohmann et al.*, 2005].

[42] The net annual mean cooling in the northern extratropics (Figure 4) is related to the strong SST response to a decrease in JJA insolation, even while there was an increase in DJF insolation. It is likely that rectification processes in the tropical Pacific lead to a more pronounced boreal winter signal than for boreal summer [*Clement et al.*, 1999]. In a similar way, the annual mean Holocene cooling in the eastern North Atlantic and Europe, contrary to the insolation signal, is related to a boreal winter phenomenon, the AO/NAO circulation pattern. The Holocene weakening of the AO/NAO is possibly driven by the tropical warming during the DJF season.

[43] Our main findings disagree with the study of *Liu et al.* [2003], which suggested that the annual mean SST changes during the early to middle Holocene were mainly caused by the annual mean insolation changes. For example, in the Arctic, the greater tilt of the Earth's axis at 7 kyr B.P. probably contributed to higher temperatures there relative to the present (preindustrial): poleward of 60°N, an increase of more than 2.5 W m^{-2} in annual mean insolation occurs. In the tropics, the net annual mean insolation decrease is less than 1 W m^{-2}, which is negligible compared to the seasonal change of more than 20 W m^{-2}.

[44] The boreal winter signal dominates the temperature response over the North Atlantic through atmospheric circulation changes. We associate the Holocene weakening of the AO/NAO pattern with the tropical warming caused by the precession-related increasing boreal winter insolation. Indeed, seasonally resolved coral data from the northern Red Sea and modeling experiments covering the last interglacial and the Holocene suggest a strong modulation of the AO/NAO by orbitally driven insolation changes [*Felis et al.*, 2004]. During the last interglacial-glacial transition (125 to 115 kyr B.P.), when eccentricity was larger and precession had a more pronounced influence on the subtropics than during the Holocene, the AO/NAO-like climate mode was dominant and its change occurred with significantly enhanced amplitude [*Felis et al.*, 2004].

5.3. Limitations

[45] For simulation by various climate models, PMIP defined the Holocene Maximum time slice to be at 6 kyr B.P. This is about a thousand years later than the northern high latitude summer insolation maximum. The reason for this definition was simply that the Laurentide and Fennoscandian continental glaciers had disappeared by then. During the last deglaciation (after the late Pleniglacial until the early Holocene, ≈15–7 kyr B.P.) the melting ice caps with their input of huge freshwater pulses into the North Atlantic caused abrupt climate changes and severe shifts in the Atlantic ocean circulation system, with global impact [*Clark et al.*, 2002]. Examples are the end of the Younger Dryas cold event at 11.5 kyr B.P. and the 8.2 kyr climate shift event [*Grootes et al.*, 1993]. In order to exclude these periods, we confined this study to the middle to late Holocene. The last 7000 years can be regarded as a relatively stable climate period compared to earlier eras and were probably free of abrupt climate shifts and rearrangements in the atmosphere-ocean system [*Fairbanks*, 1989; *Grootes et al.*, 1993; *Clark et al.*, 2002; *McManus et al.*, 2004].

[46] Accordingly, in the ensemble of Holocene simulations no noteworthy changes in the thermohaline circulation were found [*Lorenz and Lohmann*, 2004]. This mitigates the limitation that the model cannot adequately simulate fast climate transitions using the acceleration technique for the orbital forcing. Moreover, we find no indication in modeled and reconstructed data that global-

scale circulation changes are responsible for the observed surface temperature trends.

[47] The mismatch between the alkenone-derived SST data and the model results around South America (and partly southern Africa) can be taken as an indication that mechanisms other than the orbitally driven insolation changes are primarily responsible for variations in Southern Hemisphere SST, in contrast to the Northern Hemisphere. In the Southern Ocean, it is plausible that sea ice dynamics and changes in the thermohaline circulation may have significant influence on large-scale SST distribution possibly via the hemispheric seesaw effect [*Crowley*, 1992; *Stocker*, 1998; *Knorr and Lohmann*, 2003]. Owing to the acceleration technique used, these Holocene experiments could not simulate millennial-scale climate variability seen in the alkenone-derived SST records [*Rimbu et al.*, 2004]. Hence we speculate that deep ocean adjustments involving atmosphere and sea ice dynamics played a more dominant role in the Southern Hemisphere than in the Northern Hemisphere for Holocene surface temperature trends.

[48] One important component that is lacking in the ECHO-G model is a module for adaptive vegetation, since the terrestrial biosphere with its vegetation ratio, background albedo, leaf area index, etc. is prescribed. The vegetation-climate feedback almost certainly has a significant impact on climate, regionally exceeding that of the atmosphere-ocean interaction, for example, in the case of African and Asian monsoon amplification [*Texier et al.*, 2000; *Braconnot et al.*, 2002]. Therefore one of the important steps to improve the model results is to consider vegetation-climate interaction in transient climate change simulations with the ECHO-G.

[49] A large number of paleoclimate simulations have been performed utilizing so-called ''Earth system models of intermediate complexity'' (EMICs). For the sake of simulating feedbacks between as many climate components as feasible, the number of processes and the detail of description in these models are reduced [*Claussen et al.*, 2002]. For example, the atmospheric circulation may be partly parameterized [*Petoukhov et al.*, 2000; *Weber et al.*, 2004; *Renssen et al.*, 2005] or the oceanic component zonally averaged [*Petoukhov et al.*, 2000; *Crucifix et al.*, 2002]. The advantage of these models is that they include more of the components and their interactions that have a significant effect on long-term natural climate change.

[50] In the zonal mean, the magnitude of Holocene surface temperature changes of our model are in general agreement with studies using EMICs [*Crucifix et al.*, 2002; *Weber et al.*, 2004]. Notably, the experiments confirm much earlier findings [e. g., *Berger et al.*, 1990] that a considerable fraction of the climate variance is caused by orbitally driven insolation changes. However, coarse resolution or simplifications, inherent in fast running EMICs, can partly impede the simulation of important interactions like the AO/NAO climate mode. The transient simulations provided by AOGCMs account in more detail for the dynamics that are necessary to interpret the response of the climate system to the orbital forcing during the Holocene. We find that the dominant signal of orbitally induced temperature change has more regional patterns superimposed on it. Beyond the global scale, the weakening of the AO/NAO climate mode is the most important phenomenon affecting Holocene climate change.

6. Concluding Remarks

[51] The approach in this study was to compare a global Holocene proxy SST data set to results from climate model simulations with respect to changes in seasonality and global distribution patterns. We use a novel method for model acceleration regarding the orbitally driven insolation forcing in a complex circulation model [*Lorenz and Lohmann*, 2004]. With this method, a coupled atmosphere-ocean general circulation model, the ECHO-G model [*Legutke and Voss*, 1999], is able to simulate orbitally driven long-term transient climate changes.

[52] The main finding of this study is that changes in the seasonal insolation cycle during the last 7000 years of the Holocene, forced by variations in the Earth's orbital parameters, are a significant cause for the observed opposing trends of cooling and warming in the extratropics and the tropics, respectively. The spatial and seasonal heterogeneity of the simulated climate is a detailed nonlinear response of the atmosphere-ocean system to the external forcing, the seasonal and latitudinal distribution of insolation. Moreover, the similarities of the alkenone-derived and simulated SST trends strongly suggest that Holocene SST changes in the extratropics and the tropics (mainly in the Northern Hemisphere) are controlled by nonlinear changes in the entire seasonal cycle of insolation. This finding supplements the theory [*Milankovitch*, 1941; *Hays et al.*, 1976; *Imbrie et al.*, 1992] that the predominant pacemaker of long-term climate changes is primarily the orbitally driven boreal summer insolation at high northern latitudes.

[53] There has been an ongoing debate about the seasonal origin of the alkenone-derived SST signal in tropical, subtropical and high latitude regions [*Rosell-Melé et al.*, 1995; *Baumann et al.*, 1997; *Müller and Fischer*, 2001]. Our model simulations provide the possibility to compare surface temperature trends of any season to alkenone-derived SST records. In the northern high latitudes, there is better agreement of the alkenone-derived SST data with our model results during the JJA season. This suggests that high latitude alkenone-derived SST records probably reflect boreal summer conditions more than the annual mean signal. Note that the Holocene shift of the time of year of the maximum tropical insolation may have influenced the timing of coccolithophorid production and thus the trend pattern in the alkenone-derived SST data.

[54] The imprint of orbitally driven insolation forcing on Holocene surface temperature trends is dominant on a global scale but regional trend patterns are superimposed on this. In the Northern Hemisphere, changes in the AO/NAO pattern during the Holocene are detected in the simulated, as well as alkenone-derived, surface temperature patterns. The prevalent mechanisms in the Southern Hemisphere are less clear. Since long-term deep ocean adjustments could have greater influence here, orbitally driven insolation signals may not be able to dominate regional-scale changes in ocean surface waters.

[55] Our study provides a consistent interpretation of reconstructed and simulated temporal and spatial patterns of surface temperature during the middle to late Holocene. We show that temporal and spatial distribution patterns are important for the interpretation of proxy temperature trends. This study could be advantageously extended by compiling a larger global alkenone-derived SST data set, as well as adding a comprehensive compilation of other marine and land proxy data. Performing new model experiments with atmosphere-ocean-vegetation feedbacks added in the model [*Ganopolski et al.*, 1998; *Renssen et al.*, 2005] would also be an improvement.

[56] We have extended the Holocene climate simulations into the last two centuries taking into account the increase in greenhouse gases in the atmosphere [*Lorenz and Lohmann*, 2004]. The results indicate that the Northern Hemisphere summer cooling during the Holocene is of the same order of magnitude as the warming trend over the last 100 years. The extension of the model experiments into the coming centuries, so that they span the Holocene and the era of anthropogenic greenhouse gas increases, would enable the comparison of climate variability under natural and anthropogenic conditions and the investigation of differences in their characteristic temporal and spatial patterns. Such an approach could render a better assessment of future climate change.

[57] **Acknowledgments.** We would like to sincerely thank the contributors to the project GHOST (Global Holocene Spatial and Temporal Variability) as well as S. Legutke for her support concerning the ECHO-G model. Instructive comments by D. Thresher helped to improve the manuscript substantially, and discussion with and comments by A. Berger are also acknowledged. The numerical experiments have been carried out with the NEC supercomputer at the German Climate Computing Center (DKRZ). This study was funded by grants from the German Ministry of Research and Education (BMBF) through the GHOST project of the German Climate Research Program (DEKLIM). S. J. Lorenz and J.-H. Kim contributed equally to this paper.

References

Baumann, K.-H., H. Andruleit, A. Schröder-Ritzrau, and C. Samtleben (1997), Spatial and temporal dynamics of coccolithophore communites during non-production phases in the Norwegian-Greenland Sea, in *Contribution to the Micropaleontology and Paleoceanography of the Northern North Atlantic*, edited by H. C. Hass and M. A. Kaminski, *Grzybowski Found. Spec. Publ. 5*, pp. 227–243, Kraków.

Berger, A. L. (1978), Long-term variations of daily insolation and Quaternary climatic changes, *J. Atmos. Sci.*, *35*, 2362–2367.

Berger, A. L., H. Gallée, T. Fichefet, I. Marsiat, and C. Tricot (1990), Testing the astronomical theory with a coupled climate-ice-sheet model, *Palaeogeogr. Palaeoclimatol. Palaeoecol.*, *89*, 125–141.

Bertrand, C., M.-F. Loutre, and A. Berger (2002), High frequency variations of the Earth's orbital parameters and climate change, *Geophys. Res. Lett.*, *29*(18), 1893, doi:10.1029/2002GL015622.

Braconnot, P., M.-F. Loutre, B. Dong, S. Joussaume, P. Valdes, and PMIP participating groups (2002), How the simulated change in monsoon at 6 ka BP is related to the simulation of the modern climate: Results from the Paleoclimate Modeling Intercomparison Project, *Clim. Dyn.*, *19*, 107–121, doi:10.1007/s00382-001-0217-5.

Brassell, S. C., G. Eglinton, I. T. Marlowe, U. Pflaumann, and M. Sarnthein (1986), Molecular stratigraphy: A new tool for climatic assessment, *Nature*, *320*, 129–133.

Broecker, W. S. (1998), The end of the present interglacial: How and when?, *Quat. Sci. Rev.*, *17*, 689–694.

Clark, P. U., N. G. Pisias, T. F. Stocker, and A. J. Weaver (2002), The role of thermohaline circulation in abrupt climate change, *Nature*, *415*, 863–869.

Claussen, M., et al. (2002), Earth system models of intermediate complexity: Closing the gap in the spectrum of climate system models, *Clim. Dyn.*, *18*, 579–586.

Clement, A. C., R. Seager, and M. A. Cane (1999), Orbital controls on the El Niño/Southern Oscillation and the tropical climate, *Paleoceanography*, *14*, 441–456.

Conte, M. H., A. Thompson, G. Eglinton, and J. C. Green (1995), Lipid biomarker diversity in the coccolithophorid *Emiliania huxleyi* (*Prymnesiophyceae*) and the related species *Gephyrocapsa oceanica*, *J. Phycol.*, *31*, 272–282.

Crowley, T. J. (1992), North Atlantic deep water cools the Southern Hemisphere, *Paleoceanography*, *7*, 489–497.

Crowley, T. J. (2000), Causes of climate change over the past 1000 years, *Science*, *289*, 270–277.

Crucifix, M., M.-F. Loutre, P. Tulkens, T. Fichefet, and A. Berger (2002), Climate evolution during the Holocene: A study with an Earth system model of intermediate complexity, *Clim. Dyn.*, *19*, 43–60.

Etheridge, D. M., L. Steele, R. Langenfelds, R. Francey, J. Barnola, and V. Morgan (1996), Natural and anthropogenic changes in atmospheric CO_2 over the last 1000 years from air in Antarctic ice and firn, *J. Geophys. Res.*, *101*, 4115–4128.

Etheridge, D. M., L. Steele, R. Francey, and R. Langenfelds (1998), Atmospheric methane between 1000 A.D. and present: Evidence of anthropogenic emissions and climatic variability, *J. Geophys. Res.*, *103*, 15,979–15,993.

Fairbanks, R. G. (1989), A 17,000 year glacio-eustatic sea level record: Influence of glacial melting rates on the Younger Dryas event and deep ocean circulation, *Nature*, *342*, 637–642.

Felis, T., J. Pätzold, Y. Loya, M. Fine, A. H. Nawar, and G. Wefer (2000), A coral oxygen isotope record from the northern Red Sea documenting NAO, ENSO, and North Pacific teleconnections on Middle East climate variability since the year 1750, *Paleoceanography*, *15*, 679–694.

Felis, T., G. Lohmann, H. Kuhnert, S. J. Lorenz, D. Scholz, J. Pätzold, S. A. Al-Rousan, and S. M. Al-Moghrabi (2004), Increased seasonality in Middle East temperatures during the last interglacial period, *Nature*, *429*, 164–168, doi:10.1038/nature02546.

Ganopolski, A., C. Kubatzki, M. Claussen, V. Brovkin, and V. Petoukhov (1998), The influence of vegetation-atmosphere-ocean interaction on climate during the mid-Holocene, *Science*, *280*, 1916–1919.

Grootes, P. M., M. Stuiver, J. W. C. White, S. J. Johnsen, and J. Jouzel (1993), Comparison of oxygen isotope records from the GISP2 and GRIP Greenland ice cores, *Nature*, *366*, 552–554.

Guiot, J., J. Boreux, P. Braconnot, F. Torre, and PMIP Participating Groups (1999), Data-models comparison using fuzzy logic in palaeoclimatology, *Clim. Dyn.*, *15*, 569–581.

Hays, J. D., J. Imbrie, and N. J. Shackleton (1976), Variations in the Earth's orbit: Pacemaker of the ice ages, *Science*, *194*, 1121–1132.

Hewitt, C. D., and J. F. B. Mitchell (1998), A fully coupled GCM simulation of the climate of the mid-Holocene, *Geophys. Res. Lett.*, *25*, 361–364.

Hurrell, J. W. (1995), Decadal trends in the North Atlantic oscillation: Regional temperatures and precipitation, *Science*, *269*, 676–679.

Imbrie, J., et al. (1992), On the structure and origin of major glaciation cycles: 1. Linear responses to Milankovitch forcing, *Paleoceanography*, *7*, 701–738.

Indermühle, A., et al. (1999), Holocene carbon-cycle dynamics based on CO_2 trapped in ice at Taylor Dome, Antarctica, *Nature*, *398*, 121–126.

Intergovernmental Panel on Climate Change (2001), *Climate Change 2001: The Scientific Basis: Contribution of Working Group I to the Third Assessment Report of the IPCC*, edited by J. T. Houghton et al., 881 pp., Cambridge Univ. Press, New York.

Jickells, T. D., P. P. Newton, P. King, R. S. Lampitt, and C. A. Boutle (1996), Comparison of sediment trap records of particle fluxes from 19 to 48°N in the northeast Atlantic and their relation to surface water productivity, *Deep Sea Res., Part I*, *48*, 971–986.

Joussaume, S., and K. E. Taylor (2000), The Paleoclimate Modeling Intercomparison Project, in *Paleoclimate Modeling Intercomparison Project (PMIP): Proceedings of the Third PMIP Workshop, Canada, 4–8 October 1999*, edited by P. Braconnot, *WCRP-111*, pp. 9–24, World Meteorol. Organ., Geneva, Switzerland.

Kim, J.-H., and R. R. Schneider (2004), GHOST global database for alkenone-derived Holocene sea-surface temperature records, http://

www.pangaea.de/Projects/GHOST/, PANGAEA Network for Geol. and Environ. Data, Bremerhaven, Germany.

Kim, J.-H., N. Rimbu, S. J. Lorenz, G. Lohmann, S. Schouten, S.-I. Nam, C. Rühlemann, and R. R. Schneider (2004), North Pacific and North Atlantic sea-surface temperature variability during the Holocene, *Quat. Sci. Rev.*, *23*, 2141–2154, doi:10.1016/j.quascirev.2004.08.010.

Kitoh, A., and S. Murakami (2002), Tropical Pacific climate at the mid-Holocene and the Last Glacial Maximum simulated by a coupled atmosphere-ocean general circulation model, *Paleoceanography*, *17*(3), 1047, doi:10.1029/2001PA000724.

Knorr, G., and G. Lohmann (2003), Southern Ocean origin for resumption of Atlantic thermohaline circulation during deglaciation, *Nature*, *424*, 532–536.

Kohfeld, K., and S. P. Harrison (2000), How well can we simulate past climates? Evaluating the models using global palaeoenvironmental data sets, *Quat. Sci. Rev.*, *19*, 321–346.

Laskar, J., P. Robutel, F. Joutel, M. Gastineau, A. C. M. Correia, and B. Levrard (2004), A long-term numerical solution for the insolation quantities of the Earth, *Astron. Astrophys.*, *428*, 261–285, doi:10.1051/0004-6361:20041335.

Legutke, S., and R. Voss (1999), The Hamburg atmosphere-ocean coupled circulation model ECHO-G, *Tech. Rep. 18*, Dtsch. Klimarechenzentrum, Hamburg, Germany.

Liu, Z., R. G. Gallimore, J. E. Kutzbach, W. Xu, Y. Golubev, P. Behling, and R. Selin (1999), Modeling long-term climate changes with equilibrium asynchronous coupling, *Clim. Dyn.*, *15*, 325–340.

Liu, Z., E. Brady, and J. Lynch-Stieglitz (2003), Global ocean response to orbital forcing in the Holocene, *Paleoceanography*, *18*(2), 1041, doi:10.1029/2002PA000819.

Lohmann, G., and S. Lorenz (2000), The hydrological cycle under paleoclimatic conditions as derived from AGCM simulations, *J. Geophys. Res.*, *105*, 17,417–17,436.

Lohmann, G., S. J. Lorenz, and M. Prange (2005), Northern high-latitude climate changes during the Holocene as simulated by circulation models, in *The Nordic Seas: An Integrated Perspective*, *Geophys. Monogr. Ser.*, vol. 158, edited by H. Drange et al., pp. 273–288, AGU, Washington D. C.

Lorenz, S., and G. Lohmann (2004), Acceleration technique for Milankovitch type forcing in a coupled atmosphere-ocean circulation model: Method and application for the Holocene, *Clim. Dyn.*, *23*, 727–743, doi:10.1007/s00382-004-0469-y.

Lorenz, S., B. Grieger, P. Helbig, and K. Herterich (1996), Investigating the sensitivity of the atmospheric general circulation model ECHAM 3 to paleoclimatic boundary conditions, *Int. J. Earth Sci.*, *85*, 513–524.

Loutre, M. F., A. Berger, P. Bretagnon, and P.-L. Blanc (1992), Astronomical frequencies for climate research at the decadal to century time scale, *Clim. Dyn.*, *7*, 181–194.

Marchal, O., et al. (2002), Apparent long-term cooling of the sea surface in the northeast Atlantic and Mediterranean during the Holocene, *Quat. Sci. Rev.*, *21*, 455–483.

McManus, J. F., D. W. Oppo, and J. L. Cullen (1999), A 0.5-million-year record of millennial-scale climate variability in the North Atlantic, *Science*, *283*, 971–975.

McManus, J. F., R. Francois, J.-M. Gherardi, L. D. Keigwin, and S. Brown-Leger (2004), Collapse and rapid resumption of Atlantic meridional circulation linked to deglacial climate changes, *Nature*, *428*, 834–837.

Milankovitch, M. (1941), Kanon der Erdbestrahlung und seine Anwendung auf das Eiszeitenproblem, *Spec. Publ.*, *132*, 633 pp., R. Serb. Acad., Belgrade.

Müller, P. J., and G. Fischer (2001), A 4-year sediment trap record of alkenones from the filamentous upwelling region off Cape Blanc, NW Africa and a comparison with distributions in underlying sediments, *Deep Sea Res., Part I*, *48*, 1877–1903.

Müller, P. J., G. Kirst, G. Ruhland, I. von Storch, and A. Rosell-Melé (1998), Calibration of the alkenone palaeotemperature index ($U^{K'}_{37}$) based on core-tops from the eastern South Atlantic and the global ocean (60°N–60°S), *Geochim. Cosmochim. Acta*, *62*, 1757–1772.

Petoukhov, V., A. Ganopolski, V. Brovkin, M. Claussen, A. Eliseev, C. Kubatzki, and S. Rahmstorf (2000), CLIMBER-2: A climate system model of intermediate complexity. part I: Model description and performance for present climate, *Clim. Dyn.*, *16*, 1–17.

Prahl, F. G., and S. G. Wakeham (1987), Calibration of unsaturation patterns in long-chain ketone compositions for paleotemperature assessment, *Nature*, *330*, 367–369.

Renssen, H., H. Goosse, T. Fichefet, V. Brovkin, E. Driesschaert, and F. Wolk (2005), Simulating the Holocene climate evolution at northern high latitudes using a coupled atmosphere-sea ice-ocean-vegetation model, *Clim. Dyn.*, *24*, 23–43, doi:10.1007/s00382-004-0485-y.

Rimbu, N., G. Lohmann, J.-H. Kim, H. W. Arz, and R. R. Schneider (2003), Arctic/North Atlantic Oscillation signature in Holocene sea surface temperature trends as obtained from alkenone data, *Geophys. Res. Lett.*, *30*(6), 1280, doi:10.1029/2002GL016570.

Rimbu, N., G. Lohmann, S. J. Lorenz, J.-H. Kim, and R. R. Schneider (2004), Holocene climate variability as derived from alkenone sea surface temperature and coupled ocean-atmosphere model experiments, *Clim. Dyn.*, *23*, 215–227, doi:10.1007/s00382-004-0435-8.

Roeckner, E., et al. (1996), The atmospheric general circulation model ECHAM-4: Model description and simulation of the present-day climate, *Rep. 218*, Max-Planck-Inst. für Meteorol., Hamburg, Germany.

Rosell-Melé, A., G. Eglinton, U. Pflaumann, and M. Sarnthein (1995), Atlantic core-top calibration of the U^{K}_{37} index as a sea-surface palaeotemperature indicator, *Geochim. Cosmochim. Acta*, *59*, 3099–3107.

Rosell-Melé, A., et al. (2001), Precision of the current methods to measure the alkenone proxy $U^{K'}_{37}$ and absolute alkenone abundance in sediments: Results of an interlaboratory comparision study, *Geochem. Geophys. Geosyst.*, *2*(7), doi:10.1029/2000GC000141.

Sikes, E. L., J. K. Volkman, L. G. Robertson, and J.-J. Pichon (1997), Alkenones and alkenes in surface water and sediments of the Southern Ocean: Implications for paleotemperature estimation in polar regions, *Geochim. Cosmochim. Acta*, *61*, 1495–1505.

Sowers, T., R. B. Alley, and J. Jubenville (2003), Ice core records of atmospheric N_2O covering the last 106,000 years, *Science*, *301*, 945–948.

Stocker, T. F. (1998), The seesaw effect, *Science*, *282*, 61–62.

Texier, D., N. de Noblet, and P. Braconnot (2000), Sensitivity of the African and Asian monsoons to mid-Holocene insolation and data-inferred surface changes, *J. Clim.*, *13*, 164–181.

Thompson, D. W. J., and J. M. Wallace (1998), The Arctic oscillation signature in the wintertime geopotential height and temperature fields, *Geophys. Res. Lett.*, *25*, 1297–1300.

Thompson, D. W. J., and J. M. Wallace (2001), Regional climate impacts of the Northern Hemisphere Annular Mode, *Science*, *293*, 85–89.

Volkman, J. K., G. Eglinton, E. D. S. Corner, and J. R. Sargent (1980), Novel unsaturated straight-chain methyl and ethyl ketones in marine sedimens and a coccolithophore Emiliania huxleyi, *Phytochemistry*, *19*, 2619–2622.

Voss, R., and U. Mikolajewicz (2001), The climate of 6000 years BP in near-equilibrium simulations with a coupled AOGCM, *Geophys. Res. Lett.*, *28*, 2213–2216.

Weber, S. L., T. Crowley, and G. van der Schrier (2004), Solar irradiance forcing of centennial climate variability during the Holocene, *Clim. Dyn.*, *22*, 539–553, doi:10.1007/s00382-004-0396-y.

Wolff, J.-O., E. Maier-Reimer, and S. Legutke (1997), The Hamburg ocean primitive equation model HOPE, *Tech. Rep. 13*, Dtsch. Klimarechenzentrum, Hamburg, Germany.

J.-H. Kim, Centre de Formation et de Recherche sur l'Environnement Marin (CEFREM), CNRS-UMR 5110, Université de Perpignan, 52 Avenue Paul Alduy, 66860 Perpignan, Cedex, France.

G. Lohmann and N. Rimbu, Alfred-Wegener-Institut für Polar- und Meeresforschung (AWI), Bussestraße 24, D-27570 Bremerhaven, Germany.

S. J. Lorenz, Meteorologisches Institut, Universität Hamburg, Bundesstraße 55, D-20146, Hamburg, Germany. (lorenz@dkrz.de)

R. R. Schneider, Institut für Geowissenschaften, Christian-Albrechts-Universität zu Kiel, Ludewig-Meyn-Straße 10, D-24118 Kiel, Germany.